

# Sequential tunneling in doped superlattices: Fingerprints of impurity bands

Andreas Wacker and Antti-Pekka Jauho

*Mikroelektronik Centret, Bygning 345ø, Danmarks Tekniske Universitet, DK-2800 Lyngby,  
Denmark*

(December 2, 2024)

## Abstract

Electrical transport through weakly-coupled doped superlattices is investigated theoretically. For all dopings we find negative differential conductivity at sufficiently high electric fields. In low-doped samples the presence of impurity bands modifies the current-voltage characteristics substantially and we find two different current peaks whose relative height is changing with the electron temperature. These findings can explain the observation of different peaks in the current-voltage characteristics with and without external THz irradiation in low-doped samples. Furthermore this feature is suggested as a method to probe impurity bands in a transport experiment.

72.20.Ht,73.20.Dx,73.40.Gk

## I. INTRODUCTION

Perpendicular charge transport in biased superlattices is dominated by resonances due to the alignment of energy levels in different wells. These resonances yield distinct peaks in the current-voltage characteristics [1,2] associated with negative differential conductivity (NDC) at fields above the peak. The instability associated with NDC causes the formation of electric field domains [3] as well as self-sustained oscillations in such structures [4]. While for strongly coupled superlattices the electronic minibands dominate the electrical transport [5], in weakly coupled superlattices the transport is due to sequential tunneling from one well to the next. (For a discussion of the appropriate regimes see Refs. [6,7].) This situation has been already regarded in Ref. [8] for tunneling between the lowest level and excited levels in the adjacent well. There the current is driven by the different occupation of the two levels and a maximum of the current occurs when the different level are aligned. Tunneling between equivalent levels at low fields is slightly more complicated, as alignment occurs at zero field, where, of course, the current vanishes. The key point is the treatment of broadening of the states due to scattering which essentially determines the transport. This idea has been exploited to determine scattering rates by studying the transport between two quantum wells [9–11]. In the experiments [10,11] impurity scattering was diminished by the use of remote doping which enabled to study electron-electron scattering rates. In contrast to this we focus on doped superlattices in the present paper. There impurity scattering at the ionized donors is an important scattering process whose impact we will examine in the following. In a previous study [12] we have investigated a heavily doped sample and found good agreement with experimental data. Here we perform a systematic study of the low-field transport in such structures for different doping densities. We find that the formation of impurity bands [13,14] for low-doped samples causes a strong temperature dependence of the current-field relation which may display a double-peak structure at low fields.

The paper is organized as follows: Our transport model is presented in Section II. In order to understand the generic behavior we give a phenomenological approximation where many features can be seen analytically in Section III. The calculated results for different doping densities are presented in Sections IV and V using different screening models, respectively. Our calculations are compared with two different experiments concerning a highly-doped and a low-doped sample in section VI. Finally, we will discuss the general significance of our results.

## II. THE MODEL

We consider weakly coupled semiconductor quantum wells of period  $d$ . Then the electrons are essentially localized in the wells and a reasonable basis set of wave functions is given by a product of Wannier functions  $\Psi^\nu(z - jd)$  localized in well  $j$ , and plane waves  $e^{i\mathbf{k}\cdot\mathbf{r}}$ . Here the  $z$  direction is defined to be the growth direction and  $\mathbf{k}, \mathbf{r}$  are vectors within the  $(x, y)$  plane.  $\nu$  denotes the subband within the well. Here we restrict ourselves to the lowest level and omit the index  $\nu$  in the following and the energy of the lowest level is used as a reference point.

Regarding only next-neighbor coupling  $T_1$  we have the following Hamiltonian ( $F$  is the electric field, and  $e < 0$  is the charge of the electron):

$$\begin{aligned}
\hat{H} = & \sum_{j,\mathbf{k}} \left[ (E_k - jeFd) a_j^\dagger(\mathbf{k}) a_j(\mathbf{k}) \right. \\
& \left. + T_1 a_{j+1}^\dagger(\mathbf{k}) a_j(\mathbf{k}) + T_1 a_j^\dagger(\mathbf{k}) a_{j+1}(\mathbf{k}) \right] \\
& + \hat{H}^{\text{scatt}}
\end{aligned} \tag{1}$$

with the in-plane kinetic energy  $E_k = \hbar^2 k^2 / (2m_w)$ , where  $m_w$  is the effective mass in the well.  $a_j$  and  $a_j^\dagger$  are the annihilation and creation operators of electrons in well  $j$ , respectively.  $\hat{H}^{\text{scatt}}$  denotes the contribution due to scattering which is not  $\mathbf{k}$ -conserving.

Within the lowest order in the coupling  $T_1$  the current density from the lowest level in well  $j$  to the lowest level in well  $j+1$  is given by [15]

$$\begin{aligned}
J_{j \rightarrow j+1} = & \frac{2e}{A} \sum_{\mathbf{k}} |T_1|^2 \int_{-\infty}^{\infty} \frac{dE}{2\pi\hbar} A_{j+1}(\mathbf{k}, E + eFd) \\
& \times A_j(\mathbf{k}, E) [n_F(E - \mu_j) - n_F(E + eFd - \mu_{j+1})].
\end{aligned} \tag{2}$$

Here  $e$  is the electron charge,  $A$  is the sample area,  $\mu_j$  is the local chemical potential in well  $j$  measured with respect to the energy of the lowest level.  $n_F(\mathcal{E}) = 1/[1 + \exp(\mathcal{E}/k_B T)]$ , and  $T$  is the electron temperature.  $Fd$  denotes the voltage drop per period  $d$ . The spectral function  $A(\mathbf{k}, E)$  is calculated for a given intrawell scattering  $\hat{H}^{\text{scatt}}$  via the retarded self-energy  $\Sigma^{\text{ret}}(\mathbf{k}, E)$ :

$$A(\mathbf{k}, E) = \frac{-2\text{Im}\{\Sigma^{\text{ret}}(\mathbf{k}, E)\}}{(E - E_k - \text{Re}\{\Sigma^{\text{ret}}\})^2 + (\text{Im}\{\Sigma^{\text{ret}}\})^2}. \tag{3}$$

$\mu_j$  is related to the electron density  $n_j$  in well  $j$  via the relation

$$n_j = \int_{-\infty}^{\infty} dE \rho_j(E) n_F(E - \mu_j) \tag{4}$$

with the density of states

$$\rho_j(E) = \frac{2}{2\pi A} \sum_{\mathbf{k}} A_j(\mathbf{k}, E) \tag{5}$$

where the factor 2 reflects the spin degeneracy.

In our microscopic calculation we proceed as follows: First we determine the coupling  $T_1$  as well as the Wannier functions  $\Psi(z - jd)$  for the given superlattice parameters (see Appendix A). Then we calculate the self-energy  $\Sigma^{\text{ret}}(\mathbf{k}, E)$  for impurity scattering using the single-site approximation shown in Fig. 1. The respective formulas are given in appendix B. The matrix element for impurity scattering is calculated from the Coulomb potential of the individual ionized donors. Screening is treated in two different approaches, the random-phase approximation (RPA) for a free-electron gas and the Thomas-Fermi approximation (TF) using the actual density of states at the Fermi level (see appendix C). Using the calculated spectral functions  $A(\mathbf{k}, E)$  the chemical potential is determined by setting  $n_j = N_D$  in Eq. (4), where  $N_D$  is the doping density per period. Finally the current is calculated from Eq. (2). Note that all quantities used in the calculation are defined by the sample parameters and no fitting parameters are used.

### III. PHENOMENOLOGICAL DESCRIPTION

In this section we want to provide some insight into the question how scattering effects the transport. Using a constant self-energy we derive some simple expressions for the current-field relation which will help to understand the full calculations presented in subsequent sections.

As mentioned in the introduction the level broadening essentially determines the transport in the sequential limit. This can be easily seen in the limit of vanishing scattering. Then the spectral functions become  $\delta$ -functions,  $A(\mathbf{k}, E) = 2\pi\delta(E - E_k)$ . In this case the current vanishes for  $eFd \neq 0$ . (In addition further resonances may occur at finite fields, when the lowest level is aligned with higher levels in the neighboring well, which are not considered here). We rewrite Eq. (2) as follows

$$J_{j \rightarrow j+1} = e \frac{T_1^2}{\hbar} \int_{-\infty}^{\infty} dE \langle A_{j+1} \rangle(E, F) \rho_j(E) \times [n_F(E - \mu_j) - n_F(E + eFd - \mu_{j+1})] \quad (6)$$

with

$$\langle A_{j+1} \rangle(E, F) = \frac{\int_0^{\infty} dE_k A_j(\mathbf{k}, E) A_{j+1}(\mathbf{k}, E + eFd)}{\int_0^{\infty} dE_k A_j(\mathbf{k}, E)} \quad (7)$$

where we used Eq. (5) and performed the continuum limit. Now let us assume a constant self-energy  $\Sigma^{\text{ret}}(\mathbf{k}, E) = -i\Gamma/2$  in Eq. (7) for the sake of simplicity. Then the spectral functions become Lorentzians  $A(\mathbf{k}, E) = \Gamma/[(E - E_k)^2 + \Gamma^2/4]$ . Extending the lower integration to  $-\infty$  we obtain

$$\langle A_{j+1} \rangle = \frac{2\Gamma}{(eFd)^2 + \Gamma^2} \quad (8)$$

which only depends on  $F$ . Note that this simple model with a constant self-energy cannot be used in the calculation of the density of states (5) as the integral for the electron density (4) diverges in this case. Therefore we use the free-electron density of states  $\rho_j(E) = \rho_0 \Theta(E)$  (with  $\rho_0 = m/(\pi\hbar^2)$ ) and obtain for equal chemical potentials  $\mu_j = \mu_{j+1} = \mu$ :

$$J(F) = e\rho_0 \frac{T_1^2}{\hbar} \frac{2\Gamma}{(eFd)^2 + \Gamma^2} \int_0^{eFd} dE n_F(E - \mu). \quad (9)$$

For small temperature and voltage drop ( $k_B T, eFd \ll \mu$ ) we find

$$J(F) = e\rho_0 \frac{T_1^2}{\hbar} \frac{2\Gamma eFd}{(eFd)^2 + \Gamma^2} \quad (10)$$

Thus, we recover an ohmic behavior for low fields  $eFd \ll \Gamma$ , a maximum of  $J(F)$  at  $eFd = \Gamma$ , and negative differential conductivity for  $eFd > \Gamma$ . Eq. (10) has been essentially used in Refs. [10,11] for the determination of scattering rates  $\Gamma/\hbar$  from tunneling between two two-dimensional electron gases. Similar models using a phenomenological broadening  $\Gamma$  have been applied to the sequential tunneling in superlattices in Refs. [16,17]. The current at the maximum is given by

$$J_{\max} = J \left( \frac{\Gamma}{ed} \right) = e \rho_0 \frac{T_1^2}{\hbar} \quad (11)$$

which is independent of doping, scattering, and temperature in the limit of  $\mu \gg eFd, k_B T$  considered here.

If  $k_B T$  becomes of the order of  $\mu$  the factor  $\int_0^{eFd} dE n_F(E - \mu)$  in Eq. (9) is smaller than  $eFd$  and we obtain a decrease of the current with temperature. Here we have to take into account the temperature dependence of the chemical potential  $\mu$ . From Eq. (4) we find  $1 + \exp(\mu/k_B T) = \exp(n/\rho_0 k_B T)$ . This gives a zero field conductivity

$$\frac{dJ}{dF}_{|F=0} = \frac{2e^2 \rho_0}{\hbar} \frac{dT_1^2}{\Gamma} \left[ 1 - \exp \left( -\frac{n}{\rho_0 k_B T} \right) \right] \quad (12)$$

which is almost constant for  $k_B T < n/\rho_0$  and drops as  $1/k_B T$  for large temperatures.

#### IV. RESULTS FOR RPA SCREENING

As a model system we choose an  $\text{Al}_{0.3}\text{Ga}_{0.7}\text{As-GaAs}$  superlattice with barrier width  $b = 10$  nm and well width  $w = 10$  nm. We use the conduction band offset 240 meV and the effective masses  $m_w = 0.067m_e$  and  $m_b = 0.0919m_e$  [18] in the Kronig-Penney model yielding a coupling  $T_1 = -0.0116$  meV. We assume  $\delta$ -doping in the middle of the quantum wells. The interaction with impurities located in different wells is found to be negligibly small. In this section screening is treated within the RPA assuming a free-electron gas.

##### A. Density of states

In Fig. 2 we have shown the resulting densities of states for four different doping densities  $N_D$ . For high  $N_D$  the density of states exhibits a monotonic increase from  $\rho = 0$  at  $E \leq E_{\min}$  to  $\rho \sim \rho_0$  for  $E \rightarrow \infty$ , where  $E_{\min}$  denotes the lowest edge of the density of states. In contrast to this the density of states splits into two parts for small doping:  $\rho(E)$  takes finite values in a certain region below  $E = 0$ , which we will refer to as an impurity band. For higher energies  $\rho(E)$  is quite similar to the density of states of the free-electron gas. These results are in good agreement with the findings of Ref. [14]. The onset of the impurity band occurs at slightly larger energies  $E_{\min}$  here, as the wavefunctions are less confined due to the spreading into the barrier which was neglected in Ref. [14].

We also marked the positions of the Fermi level  $E^F$  (i.e., the chemical potential for  $T = 0$ ). For low densities the position is just in the middle of the impurity band, indicating that the impurity band consists of exactly two states per impurity due to the assumed spin degeneracy. (This degeneracy would be lifted if spin-resolved interaction was taken in account, see also appendix B.) For high densities the position of  $E^F$  roughly equals the Fermi level of the free-electron gas  $N_D/\rho_0$ . The crossover between these two limits occurs at  $N_D \approx 5 \cdot 10^{10}/\text{cm}^2$  where  $E^F \approx 0$ .

The respective spectral functions are plotted in Fig. 3. For  $E = 5$  meV  $A(k, E)$  resembles a Lorentzian centered close to  $E_k \approx E$ . This is the generic behavior of a free quasiparticle with a finite lifetime due to scattering. The width of the spectral functions is increasing

with doping due to the enhanced scattering. We find a full width at half maximum  $\Gamma = 0.5$  meV for  $N_D \approx 1 \cdot 10^{10}/\text{cm}^2$  and  $\Gamma = 5$  meV for  $N_D \approx 1 \cdot 10^{11}/\text{cm}^2$ , which are in the range of the calculated values of  $-2\text{Im}\{\Sigma(\mathbf{k}, E)\}$ .

For  $E = -5$  meV the spectral functions exhibit a monotonic decrease. For high doping the slope is comparable to the slope at  $E = 5$  meV. In contrast to this, the spectral function for  $E = 5$  meV and  $E = -5$  meV are entirely different for low doping, indicating that two different types of states occur. While the states for  $N_D = 10^{10}/\text{cm}^2$  are essentially free-particle states at  $E = 5$  meV, they are localized in space for  $E = -5$  meV, which is the signature of an impurity band [13].

## B. Currents

We calculate the current densities  $J_{j \rightarrow j+1}(eFd)$  for different electron temperatures  $T$  from Eq. (2). The results are shown in Fig. 4. For all temperatures and densities we find an ohmic range for low electric fields and negative differential conductance for high electric fields. Let us first regard the high doping case (a-c), where no impurity bands form and the Fermi level is significantly above  $E = 0$ . In this case the approximation (9) is justified and indeed we find a maximum at values of  $eFd$  which are in the range of calculated values of  $\Gamma = -2\text{Im}\{\Sigma^{\text{ret}}(\mathbf{k}, E)\}$ . The height is estimated by  $J_{\max} = 0.91\text{A}/\text{cm}^2$  from Eq. (11) which is in good agreement with the full calculation at  $T = 4$  K. Note that the maximal current is almost independent on the doping in this range. For  $N_D = 5 \cdot 10^{11}/\text{cm}^2$  the chemical potential is larger than  $k_B T$  for all temperatures. Thus, the current is hardly affected by the temperature. In contrast to this the current drops with temperature for lower doping ( $N_D = 10^{11}/\text{cm}^2$ ). All these findings are in good agreement with the phenomenological description using a constant  $\Gamma$  discussed above.

For the low-doped samples (see Figs. 4(e,f)) an entirely new scenario occurs. Here we find two different maxima in the current-field relation whose relative weight is changed by temperature. The reason for this behavior is the presence of impurity bands for these doping levels. For  $T = 4$  K we find a maximum at  $eF_{\text{high}}d \approx 8$  meV. This is due to tunneling from the impurity band to the free states (see Fig. 5(a)). The maximum occurs at the energy where the bottom of the impurity band in one well is aligned with the band edge of the free-electron states in the neighboring well, i.e.,  $eF_{\text{high}}d \approx |E_{\min}|$ . An increasing temperature leads to a transfer of electrons from the impurity band to the free-electron states and consequently the current at  $eF_{\text{high}}d$  decreases with increasing  $T$ . The density of states in the impurity band is much lower than in the free-electron states, and hence the majority of the electrons will be in the free-electron states for  $k_B T \gtrsim |E_{\min}|$  (see Fig. 5(b) where the grey scale denotes the relative occupation). The current contribution due to the free-electron states can be understood within the phenomenological constant- $\Gamma$  approach. There is a maximum at  $eF_{\text{low}}d \approx \Gamma$ , which coincides with the full width at half maximum of the spectral function at  $E = 5$  meV in Fig. 3. The amplitude of this maximum depends on two competing effects: On the one hand the occupation of the free-electron states increases with temperature. On the other hand the Fermi-factor in Eq. (9) strongly decreases with temperature. This explains the calculated behavior, where the peak at  $eF_{\text{low}}d$  takes its maximum at intermediate temperatures.

## V. RESULTS FOR THOMAS-FERMI SCREENING

The properties related with the formation of impurity bands are sensitive to the actual screening of the interaction [13]. For low doping densities the density of states differs essentially from the free-electron density of states and thus the use of RPA-screening by a free-electron gas is questionable. In order to take this effect into account we use the Thomas-Fermi approximation (TF) with the actual density of states at the Fermi level (see appendix C) in this section. Of course neither the free-electron RPA nor the TF approximation treat the screening entirely correct, but we hope to obtain some insight into the general features by comparing these two approaches.

In Fig. 6 we show the resulting density of states which is in qualitative agreement with the results of the RPA screening (Fig. 2). For  $N_D = 5 \cdot 10^{11}/\text{cm}^2$  the density of states is almost identical while for lower densities some deviations occur. Especially the onset of the impurity band  $E_{\min}$  is shifted to lower energies for TF-screening. Furthermore the impurity bands extend over a larger energy range and have a lower density of states, so that the total density is conserved. The reason for these deviations lies in the fact that TF-screening is less effective than RPA screening if the actual density of states at the Fermi level is used. Therefore both the binding energy of the impurities as well as the broadening of the states becomes larger.

This manifests itself in the calculated current densities (see Fig. 7). For high doping (a) the characteristics are almost identical, while for lower doping deviations occur. At first note that the maxima due to tunneling between free-electron states (the maximum for  $N_D = 10^{11}/\text{cm}^2$  as well as the maxima  $F_{\text{low}}$  for  $N_D = 2 \cdot 10^{10}/\text{cm}^2$  and  $N_D = 10^{10}/\text{cm}^2$ ) are shifted to the right according to the stronger scattering which increases  $\Gamma$ . At second the peak at  $F_{\text{high}}$  is shifted to the right compared to Fig. 4. Again we find  $eF_{\text{high}}d \approx E_{\min}$  for both densities.

Therefore we conclude that within both approximations for screening the two maxima are determined by specific quantities describing the scattering.  $eF_{\text{low}}d$  reflects the average broadening  $\Gamma$  of the free-particle states and  $eF_{\text{high}}d$  is the energy separation between the onset of the impurity band and the free-particle states.

## VI. COMPARISON WITH EXPERIMENTS

Previously [12], we have applied our formalism for the highly-doped sample ( $N_D = 8.75 \cdot 10^{11}/\text{cm}^2$ ) of Refs. [19,20]. There we found good quantitative agreement with the experimental data, albeit we had to assume a barrier width which was slightly smaller than the nominal value. The position of the first maximum occurred at  $eFd = 13$  meV, which is almost independent of the barrier width (which mainly changes  $T_1$ ) and in excellent agreement with the experimental finding. The second resonance, as well as the formation of field domains was also studied in Ref. [12], and again good agreement with experimental data was found.

A low-doped superlattice ( $N_D = 6 \cdot 10^9/\text{cm}^2$ ) was used in the experiments of Refs. [21,22]. Here the current-voltage characteristic was measured both with and without irradiation by a free-electron laser. Without irradiation a broad maximum was found in the range  $50 \text{ mV} < U < 100 \text{ mV}$  where the current is almost constant. For  $U > 100 \text{ mV}$  domain

formation sets in. Dividing by the number of periods ( $N = 10$ ), the maximum extends to  $eF_{\text{unirr}}d \approx 10$  meV. In contrast to this, the photon-replica under strong THz-irradiation could be consistently explained by assuming an “instantaneous” current-voltage characteristic [22] with a distinct maximum at  $U \approx 20$  mV (i.e.,  $eF_{\text{irr}}d = 2$  meV).

Now we calculate the current-field relation for this superlattice using the experimental sample parameter  $b = 5$  nm,  $w = 15$  nm,  $A = 8\mu\text{m}^2$ . In order to model the homogeneous doping we use 8 equally spaced  $\delta$ -doping layers per period. The calculated density of states for both RPA and TF screening is shown in Fig. 8. The density of states resembles the result for low doping found before. Nevertheless we do not find a separation between the impurity band and the free-particle states. The reason is the homogeneous doping: The different impurity positions have different binding energies which smears the impurity band. Again the onset of the impurity band occurs at significantly lower energies within the reduced Thomas-Fermi screening. Both values of  $|E_{\text{min}}|$  are smaller than the corresponding values for low doping for the calculation done before (see Figs. 2,6). This is due to the larger well width in the sample [22]: The Wannier-states are less localized and therefore the matrix-element for impurity scattering(B2) as well as the binding energy of the impurity levels is smaller.

The results for the current-field relation is shown in Fig. 9. Again we find two maxima whose relative height changes with temperature. The position of the maximum for low temperatures,  $eF_{\text{high}}d$ , is almost identical to the value of  $|E_{\text{min}}|$  for both types of screening like in the calculations shown before.

Now we can offer an explanation for the two different maxima occurring in the experiment [21,22] with and without irradiation mentioned above. For low electron temperatures and without irradiation the maximum at  $eF_{\text{high}}d$  dominates the transport and thus domain formation sets in at voltages exceeding  $U \approx NeF_{\text{high}}d$  where  $N = 10$  is the number of wells. If the THz radiation is present the electrons are excited from the impurity band into the free-electron states corresponding to a larger effective electron temperature. Thus, the maximum at  $U = NeF_{\text{low}}d$  is dominant, and the photon replicas corresponding to this feature are seen experimentally. The experimental values therefore suggest  $eF_{\text{high}}d = 10$  meV and  $eF_{\text{low}}d = 2$  meV which is in excellent agreement with the calculation using Thomas-Fermi screening. Note that also the height of the current is in the range of the measured currents  $\approx 0.6\mu\text{A}$ .

As a further test of the theory, we next consider the temperature dependence of the zero-bias conductance  $G = dI/dU$ . The results are shown in Fig. 10 both for our full calculation using TF-screening as well as for spectral functions calculated within the self-consistent Born-approximation(B7) where no impurity bands form. In the latter case  $G$  is monotonously decreasing in  $T$  as shown in Fig. 10. This can be easily understood within the phenomenological constant- $\Gamma$  approach(12). However, a different scenario emerges if the electrons occupy impurity bands for low temperatures. Then  $G$  is strongly suppressed due to the small values of  $A(\mathbf{k}, E)$  for  $E < 0$ , see Fig. 3. As temperature is increased, more electrons are excited to the free-electron states, and  $G$  *increases* with  $T$  until the impurity bands are almost empty at  $k_B T \sim |E_{\text{min}}|$ . This physical picture is confirmed by the experimental data shown in Fig. 10. At low temperatures the agreement is quantitative, while at intermediate  $T$  the theory overestimates  $G$ ; this is most likely due to additional scattering processes not included in our calculation, or by the presence of a contact resistance which may limit the

experimental conductance.

Thus we may conclude that the results of our calculations are in good agreement with existing experimental data both for high and low doping. Nevertheless, a direct observation of the two-peak structure is not available so far.

## VII. DISCUSSION

We have presented calculations for the electrical transport in weakly-coupled doped superlattices, where the transport is given by sequential tunneling. We find negative differential conductance for all doping densities and temperatures for sufficiently large electric fields. This will give rise to instabilities leading to domain formation [23,24] or self-sustained current oscillations [4]. Within the full transport model using Eq. (2) these effects are discussed in Ref. [7].

For high doping  $N_D \gtrsim 10^{11}/\text{cm}^2$  or high temperatures  $k_B T \gtrsim |E_{\min}|$  the electrons mainly occupy free quasiparticle states. Then the general behavior can be understood within a phenomenological model using a constant self-energy  $-i\Gamma/2$ . The current exhibits a maximum at  $eFd \approx \Gamma$  which can be used to investigate scattering processes. For doped samples impurity scattering is an important scattering process which we considered here. The inclusion of further scattering processes like interface roughness scattering, electron-electron scattering, or phonon scattering will increase  $\Gamma$  and therefore the position of the first peak.

For low-doped samples  $N_D \ll 10^{11}/\text{cm}^2$  and low temperatures  $k_B T \ll |E_{\min}|$  the presence of impurity bands influences significantly the low-field transport. Then a second maximum at  $eF_{\text{high}}d \approx |E_{\min}|$  occurs. This maximum provides a possibility to obtain information about the position of the impurity band. This position depends strongly on the screening as can be seen by comparison of the calculations within RPA and TF. Therefore such experiments could serve as a test on various models for screening. In this sense the results from Ref. [22] suggest that the screening within the free-particle RPA might be too strong for low-doped samples although this result is not totally conclusive as the two peak structure could not be directly resolved. Furthermore it would be interesting to see if effects due to spin splitting of the impurity band are visible in experiments. These experiments can be both carried out in doped superlattices as well as in resonant tunneling between neighboring two-dimensional electron gases in the spirit of Ref. [10,11]. The latter has the advantage that problems due to domain formation in the region of negative differential conductivity do not occur. An important aspect in such experiments is the problem of electron heating as the temperature  $T$  refers to the temperature of the electronic distribution. In order to avoid heating, structures with thick barriers should be used where the Joule heating becomes small.

## ACKNOWLEDGMENTS

We want to thank Ben Hu for helpful discussions as well as J. Allen and Stefan Zeuner for bringing our attention to the low-doped samples and providing unpublished data. A.W. acknowledges financial support by the Deutsche Forschungsgemeinschaft.

## APPENDIX A: CALCULATION OF THE TRANSITION ELEMENTS

In a superlattice structure the coupling between neighboring wells  $T_1$  is related to the dispersion relation  $E(q)$  of the miniband (see [7]) via

$$T_1 = \frac{d}{2\pi} \int_{-\pi/d}^{\pi/d} dq E(q) e^{iqd}. \quad (\text{A1})$$

For a next-neighbor tight-binding model we have  $E(q) = -(\Delta/2) \cos(qd)$  and  $T_1$  is equal to a fourth of the miniband width  $\Delta$ . Here we calculate  $E(q)$  for a given superlattice via the Kronig-Penney model for the respective sample parameters. Furthermore we determine the Wannier-functions  $\Psi(z - jd)$  localized in well  $j$  from the Bloch-functions  $\phi_q(z)$ . These Wannier-functions are used for the calculation of the matrix elements for scattering.

## APPENDIX B: CALCULATION OF THE SELF-ENERGIES

We assume that the electron density is provided by doping of the superlattice. Thus, scattering at ionized impurities is an important scattering process. In addition there may be interface roughness scattering, phonon scattering, or electron-electron scattering, which we will neglect in the following. For weakly coupled superlattices, the dominating scattering process occurs within the wells, which are assumed to be identical. Thus, the well index  $j$  can be omitted. Scattering at the ionized impurities is described by the Hamiltonian

$$\hat{H}^{\text{scatt}} = \frac{1}{A} \sum_{\mathbf{k}, \mathbf{p}, \alpha} V_\alpha(\mathbf{p}) a^\dagger(\mathbf{k} + \mathbf{p}) a(\mathbf{k}) \quad (\text{B1})$$

where the subscript  $\alpha$  denotes the impurity located at the position  $(\mathbf{r}_\alpha, z_\alpha)$ . The matrix element is calculated with the Wannier functions yielding:

$$\begin{aligned} V_\alpha(\mathbf{p}) &= \int d^2r dz e^{-i\mathbf{p}\cdot\mathbf{r}} \Psi^*(z) \Psi(z) \\ &\quad \times \frac{-e^2}{4\pi\epsilon_s\epsilon_0\sqrt{|\mathbf{r} - \mathbf{r}_\alpha|^2 + (z - z_\alpha)^2}} \\ &= \frac{-e^2}{2\epsilon_s\epsilon_0 p} \int dz \Psi^*(z) \Psi(z) e^{-p|z - z_\alpha|} e^{-i\mathbf{p}\cdot\mathbf{r}_\alpha}. \end{aligned} \quad (\text{B2})$$

Using the bare Coulomb interaction  $V_\alpha(\mathbf{p})$  the relevant integrals in the self-energies are divergent. Thus screening is essential for the calculation. We treat screening within the Random-Phase approximation (RPA) of the free-electron gas as well as within an effective Thomas Fermi approximation (TF) (see appendix C). With the screened impurity potential  $V_\alpha^{\text{sc}}(\mathbf{p}) = V_\alpha(\mathbf{p})/\epsilon(\mathbf{p})$  the self-energy is calculated within the self-consistent single-site approximation (shown diagrammatically in Fig. 1) like in Ref. [13]. Then the self-energy contribution from the impurity  $\alpha$  is given by

$$\Sigma_\alpha(\mathbf{k}, E) = \frac{1}{A^2} \sum_{\mathbf{k}_1} V_\alpha^{\text{sc}}(\mathbf{k} - \mathbf{k}_1) G(\mathbf{k}_1, E) V_\alpha^{\text{sc}}(\mathbf{k}_1 - \mathbf{k})$$

$$\begin{aligned}
& + \frac{1}{A^3} \sum_{\mathbf{k}_1, \mathbf{k}_2} V_\alpha^{\text{sc}}(\mathbf{k} - \mathbf{k}_1) G(\mathbf{k}_1, E) V_\alpha^{\text{sc}}(\mathbf{k}_1 - \mathbf{k}_2) \\
& \quad \times G(\mathbf{k}_2, E) V_\alpha^{\text{sc}}(\mathbf{k}_2 - \mathbf{k}) \\
& + \dots
\end{aligned} \tag{B3}$$

where  $G(\mathbf{k}, E) = (E - E_k - \Sigma^{\text{ret}}(\mathbf{k}, E))^{-1}$  is the full retarded Green function and

$$\Sigma^{\text{ret}}(\mathbf{k}, E) = \sum_\alpha \Sigma_\alpha(\mathbf{k}, E) \tag{B4}$$

is the sum over all contributions. In case of  $\delta$ -doping the impurity potentials(B2) from different impurities located in the same well differ only by a phase factor and the sum over  $\alpha$  can be replaced by a multiplication with the number of impurities per layer  $N_D A$ . Eq. (B3) can be transformed to the self-consistent equation (see, e.g., [13])

$$\begin{aligned}
K_\alpha(\mathbf{k}_1, \mathbf{k}, E) &= V_\alpha^{\text{sc}}(\mathbf{k}_1 - \mathbf{k}) \\
& + \frac{1}{A} \sum_{\mathbf{k}_2} V_\alpha^{\text{sc}}(\mathbf{k}_1 - \mathbf{k}_2) G(\mathbf{k}_2, E) K_\alpha(\mathbf{k}_2, \mathbf{k}, E)
\end{aligned} \tag{B5}$$

which we solve numerically for a given self-energy function  $\Sigma^{\text{ret}}(\mathbf{k}, E)$  entering  $G(\mathbf{k}_2, E)$ . We parametrize  $\mathbf{k}_1, \mathbf{k}$  by  $E_{k_1}, E_k$ , and  $\phi = \angle(\mathbf{k}_1, \mathbf{k})$  and discretize the resulting equation. This gives a set of linear equations for the components of  $K(E_{k_1}, \phi)$  which is solved by matrix inversion. Then the self-energy reads:

$$\Sigma_\alpha(\mathbf{k}, E) = \frac{1}{A^2} \sum_{\mathbf{k}_1} V_\alpha^{\text{sc}}(\mathbf{k}_1 - \mathbf{k}) G(\mathbf{k}_1, E) K_\alpha(\mathbf{k}_1, \mathbf{k}, E). \tag{B6}$$

The equations (B4,B5,B6) have to be solved selfconsistently thus determining the self-energy  $\Sigma^{\text{ret}}(\mathbf{k}, E)$ .

Our single-site-approximations neglects all contributions from crossed diagrams as well as the spin-resolved electron-electron interaction leading to the splitting of the impurity bands (the Mott transition, see e.g. [25]). The latter may become important for very low densities when the impurity bands are narrow. Finally note that within this approximation for  $\Sigma^{\text{ret}}(\mathbf{k}, E)$  the integral (4) is a well defined quantity, as  $\text{Im}\{\Sigma^{\text{ret}}(\mathbf{k}, E)\} = 0$  (and thus  $A(\mathbf{k}, E) = 0$ ) for  $E < E_{\min}$ .

Finally note that no impurity bands are found within the self-consistent Born approximation

$$\Sigma_\alpha(\mathbf{k}, E) = \frac{1}{A^2} \sum_{\mathbf{k}_1} V_\alpha^{\text{sc}}(\mathbf{k} - \mathbf{k}_1) G(\mathbf{k}_1, E) V_\alpha^{\text{sc}}(\mathbf{k}_1 - \mathbf{k}) \tag{B7}$$

which is just the first diagram from Fig. 1.

## APPENDIX C: THE SCREENING

In order to consider screening we have to include the electron-electron interaction given by the Hamiltonian

$$\hat{H}^{ee} = \frac{1}{2A} \sum_{\mathbf{k}, \mathbf{k}', \mathbf{p}} W(\mathbf{p}) a^\dagger(\mathbf{k} + \mathbf{p}) a^\dagger(\mathbf{k}' - \mathbf{p}) a(\mathbf{k}') a(\mathbf{k}). \quad (C1)$$

where the matrix element is calculated by

$$W(\mathbf{p}) = \frac{e^2}{2\epsilon_s \epsilon_0 p} \int dz_1 \int dz_2 \Psi^*(z_1) \Psi^*(z_2) \times \Psi(z_2) \Psi(z_1) e^{-p|z_1-z_2|}. \quad (C2)$$

Within the random-phase approximation (RPA) the screening is described by [15]

$$V_\alpha^{\text{RPA}}(\mathbf{p}) = \frac{V_\alpha(\mathbf{p})}{1 - \Pi^0(\mathbf{p}, \omega = 0) W(\mathbf{p})}. \quad (C3)$$

For a free-electron gas the two-dimensional vacuum polarizability  $\Pi^0(\mathbf{p}, \omega = 0)$  for  $T = 0$  is given by [26]

$$\Pi^0(\mathbf{p}, \omega = 0) = -\rho_0 \left( 1 - \Theta(p - 2k_F) \sqrt{1 - 4 \frac{k_F^2}{p^2}} \right). \quad (C4)$$

where  $k_F = (2\pi N_D)^{1/2}$  is the Fermi wave-vector.

Actually, the electronic states are affected by the impurity scattering, which may change the density of states dramatically as can be seen from Fig. 2. Now the polarizability  $\Pi(p = 0)$  is related to the *actual density of states* at the chemical potential which is significantly lower than  $\rho_0$ . Calculations within the Born-approximation show that the  $p$ -dependence of the polarizability becomes weaker and that  $\Pi(0)$  decreases with increasing scattering [27,28]. In order to accommodate these trends we make the replacement  $\Pi^0(k) \rightarrow \Pi^*(k) = -\rho(E^F)$ , given by the calculated density of states of Fig. 2 and the chemical potential at  $T = 0$ . Then we obtain the screened impurity interaction

$$V_\alpha^{\text{TF}}(\mathbf{p}) = \frac{V_\alpha(\mathbf{p})}{1 + \rho(E^F) W(\mathbf{p})}. \quad (C5)$$

This is equivalent to the Thomas-Fermi approximation for the screening. The same type of screening has been considered in Ref. [13] as well. Of course both ways of including screening are approximations. In a full calculation the scattering has to be treated self-consistently in the calculation of the polarizability. Such a calculation was performed in Ref. [29] for a quantum wire within the restriction of a delta-potential for impurity scattering.

Here we restricted ourselves both to screening and scattering within the same well. The extension to screening by electrons from neighboring wells is given in Ref. [7]. The results are almost indistinguishable for the sample discussed here due to the relatively large barrier width. The temperature dependence of the screening is neglected in all calculations.

## REFERENCES

- [1] L. Esaki and L. L. Chang, Phys. Rev. Lett. **33**, 495 (1974).
- [2] F. Capasso, K. Mohammed, and A. Y. Cho, Appl. Phys. Lett. **48**, 478 (1986).
- [3] S. H. Kwok, H. T. Grahn, M. Ramsteiner, K. Ploog, F. Prengel, A. Wacker, E. Schöll, S. Murugkar, and R. Merlin, Phys. Rev. B **51**, 9943 (1995) and references cited therein.
- [4] J. Kastrup, R. Hey, K. H. Ploog, H. T. Grahn, L. L. Bonilla, M. Kindelan, M. Moscoso, A. Wacker, and J. Galán, Phys. Rev. B **55**, 2476 (1997).
- [5] L. Esaki and R. Tsu, IBM J. Res. Develop. **14**, 61 (1970).
- [6] B. Laikhtman and D. Miller, Phys. Rev. B **48**, 5395 (1993).
- [7] A. Wacker, in *Theory of transport properties of semiconductor nanostructures*, edited by E. Schöll (Chapman and Hall, London, 1997), in print (cond-mat/9701105).
- [8] R. F. Kazarinov and R. A. Suris, Sov. Phys. Semicond. **6**, 120 (1972).
- [9] L. Zheng and A. H. MacDonald, Phys. Rev. B **47**, 10619 (1993).
- [10] S. Q. Murphy, J. P. Eisenstein, L. N. Pfeiffer, and K. W. West, Phys. Rev. B **52**, 14825 (1995).
- [11] N. Turner, J. T. Nicholls, E. H. Linfield, K. M. Brown, G. A. C. Jones, and D. A. Ritchie, Phys. Rev. B **54**, 10614 (1996).
- [12] A. Wacker and A.-P. Jauho, Physica Scripta **T69**, 321 (1997).
- [13] A. Gold, J. Serre, and A. Ghazali, Phys. Rev. B **37**, 4589 (1988).
- [14] J. Serre, A. Ghazali, and A. Gold, Phys. Rev. B **39**, 8499 (1989).
- [15] G. D. Mahan, *Many-Particle Physics* (Plenum, New York, 1990).
- [16] D. Miller and B. Laikhtman, Phys. Rev. B **50**, 18426 (1994).
- [17] R. Aguado, G. Platero, M. Moscoso, and L. L. Bonilla, preprint cond-mat/9703131.
- [18] *Properties of Aluminium Gallium Arsenide*, edited by S. Adachi (INSPEC, London, 1993).
- [19] P. Helgesen and T. G. Finstad, in *Proceedings of the 14<sup>th</sup> Nordic Semiconductor Meeting*, edited by O. Hansen (University of Århus, Århus, 1990), p. 323.
- [20] P. Helgesen, T. G. Finstad, and K. Johannessen, J. Appl. Phys. **69**, 2689 (1991).
- [21] B. J. Keay, S. Zeuner, S. J. Allen, K. D. Maranowski, A. C. Gossard, U. Bhattacharya, and M. J. M. Rodwell, Phys. Rev. Lett. **75**, 4102 (1995).
- [22] S. Zeuner, B. J. Keay, S. J. Allen, K. D. Maranowski, A. C. Gossard, U. Bhattacharya, and M. J. W. Rodwell, Phys. Rev. B **53**, 1717 (1996).
- [23] F. Prengel, A. Wacker, and E. Schöll, Phys. Rev. B **50**, 1705 (1994), ibid **52**, 11518 (1995).
- [24] L. L. Bonilla, J. Galán, J. A. Cuesta, F. C. Martínez, and J. M. Molera, Phys. Rev. B **50**, 8644 (1994).
- [25] B. I. Shklovskii and A. L. Efros, *Electronic Properties of Doped Semiconductors* (Springer, Berlin, 1984).
- [26] F. Stern, Phys. Rev. Lett. **18**, 546 (1967).
- [27] T. Ando, J. Phys. Soc. Jpn. **51**, 3215 (1982).
- [28] S. Das Sarma, Phys. Rev. Lett. **50**, 211 (1983).
- [29] B. Y. Hu and S. Das Sarma, Phys. Rev. B **48**, 5469 (1993).

## FIGURES

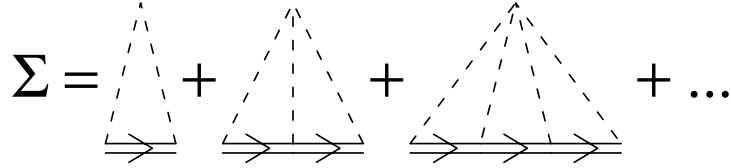


FIG. 1. The self-consistent single-site approximation. The dashed lines indicate impurity potentials and the double lines denote the full Green-function

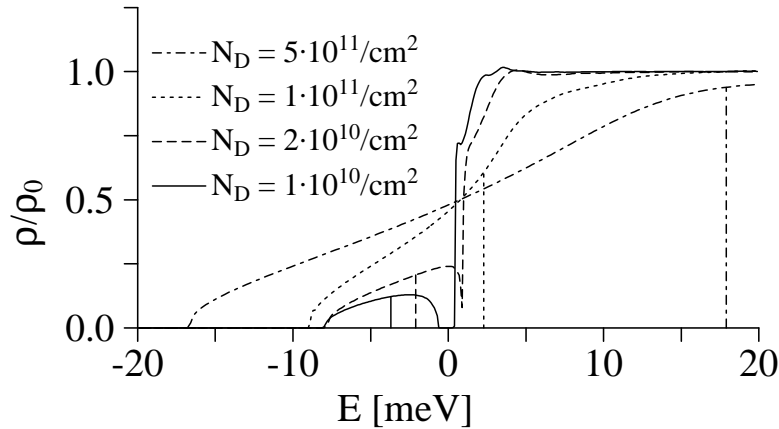


FIG. 2. Calculated density of states in units of the 2D free carrier density  $\rho_0$  using RPA screening. The vertical lines indicate the position of the chemical potential for  $T = 0$  at the respective doping densities.

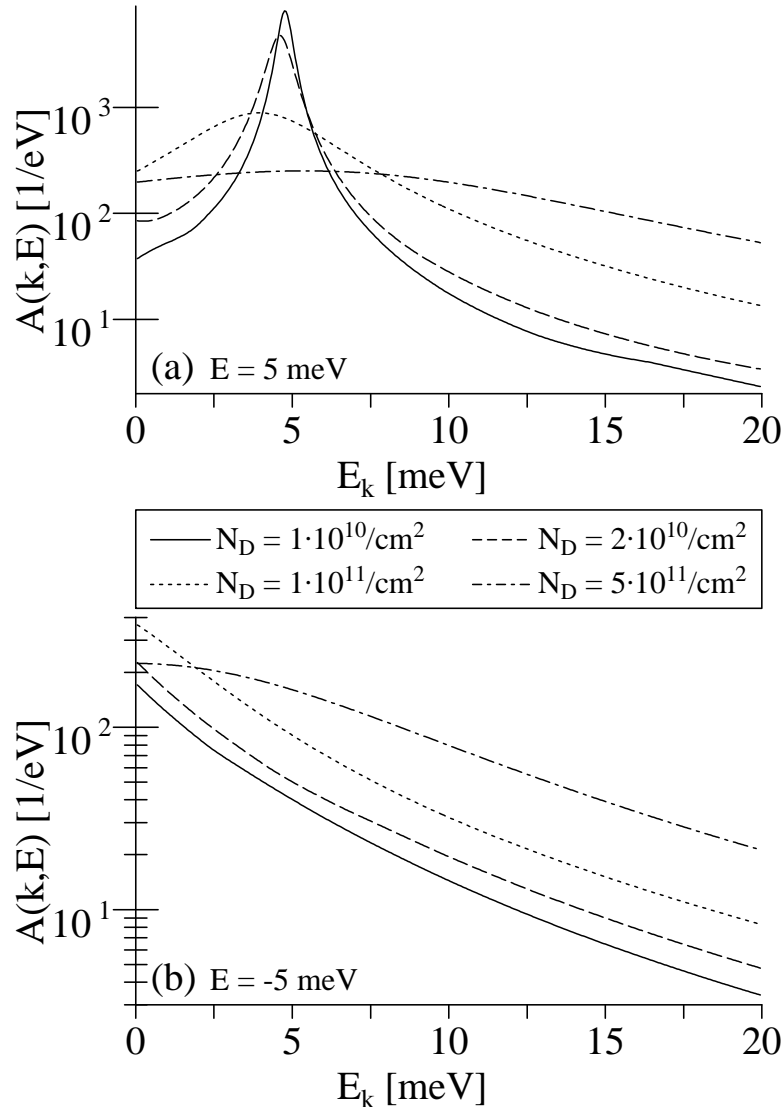


FIG. 3. Calculated spectral functions  $A(E, k)$  versus  $E_k = \hbar^2 k^2 / 2m$  using RPA screening for different doping densities at  $E = 5 \text{ meV}$  (a) and  $E = -5 \text{ meV}$  (b).

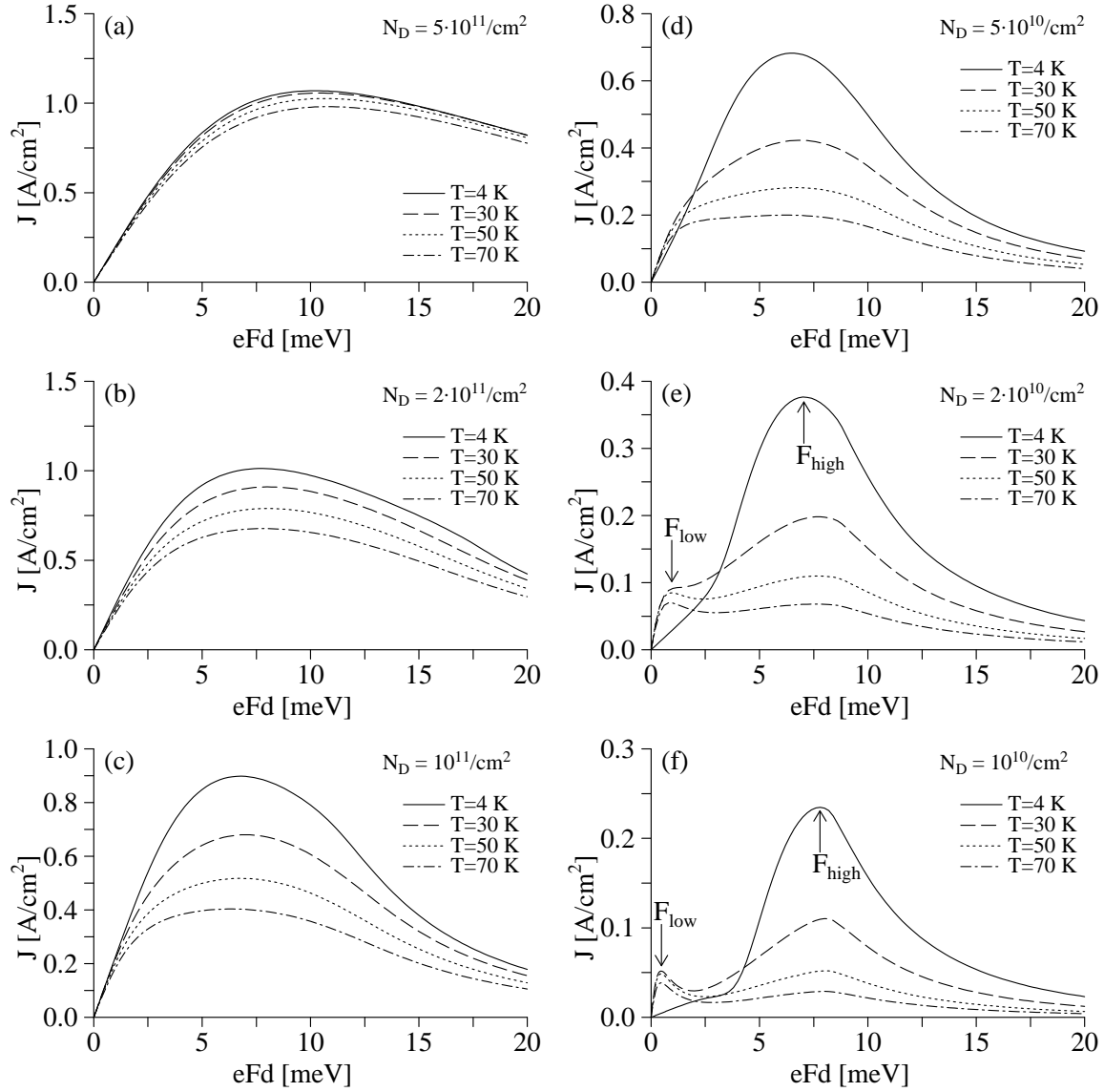


FIG. 4. Calculated temperature dependence of the current-field relations for different doping densities. The screening is treated within the RPA.

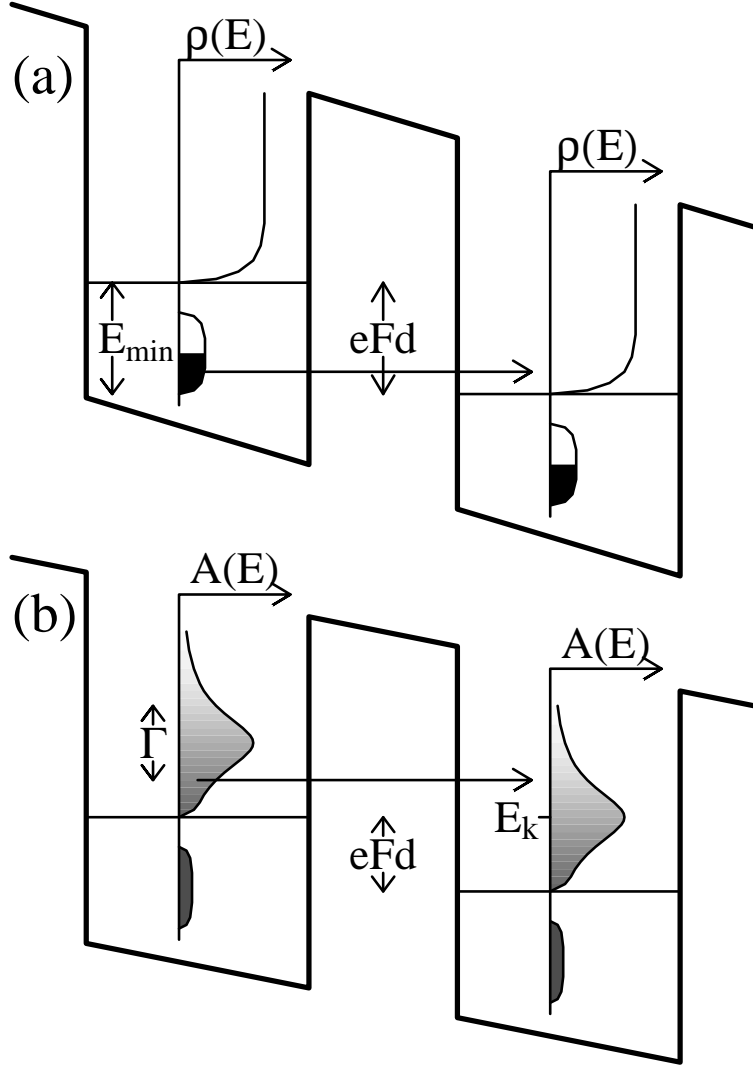


FIG. 5. Explanation of the two different current maxima within a sketch of the conduction band profile: (a) For low temperatures the electrons occupy the impurity band (black area). As these states exhibit a flat spectral function (see Fig. 3(b)) they contain contributions from essentially all  $\mathbf{k}$ -vectors and thus tunneling into the free-particle states is possible at all energies. Maximal current is found when all states from the impurity band can tunnel into the free-particle states, i.e.,  $eFd \approx |E_{\min}|$ . (b) For high temperatures the electrons occupy the free-electron states as well (the grey scale indicates the occupation given by the Fermi-function). The spectral function  $A(\mathbf{k}, E)$  of such a free-electron state with given wave vector  $\mathbf{k}$  is peaked around  $E = E_k$  as shown in the figure. Due to  $\mathbf{k}$ -conservation tunneling can only take place if the spectral functions for the same  $\mathbf{k}$  of both wells overlap. On the other hand a net current is caused by the difference in occupation. This competition results in a current maximum for  $eFd \approx \Gamma$  as shown in section III.

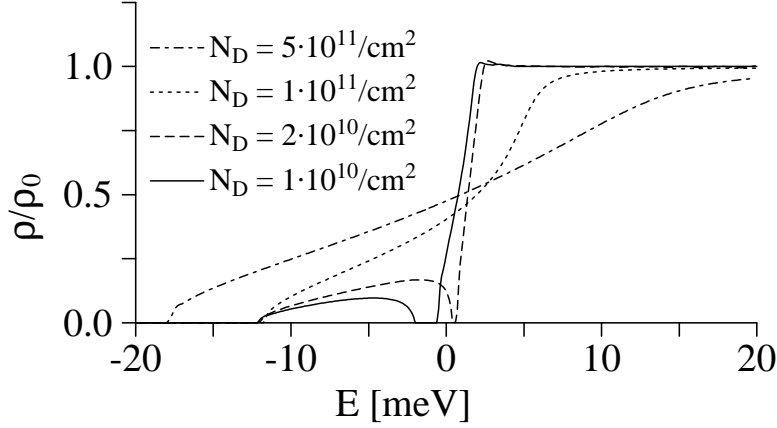


FIG. 6. Calculated density of states in units of the 2D free carrier density  $\rho_0$  using Thomas-Fermi screening for different doping densities.

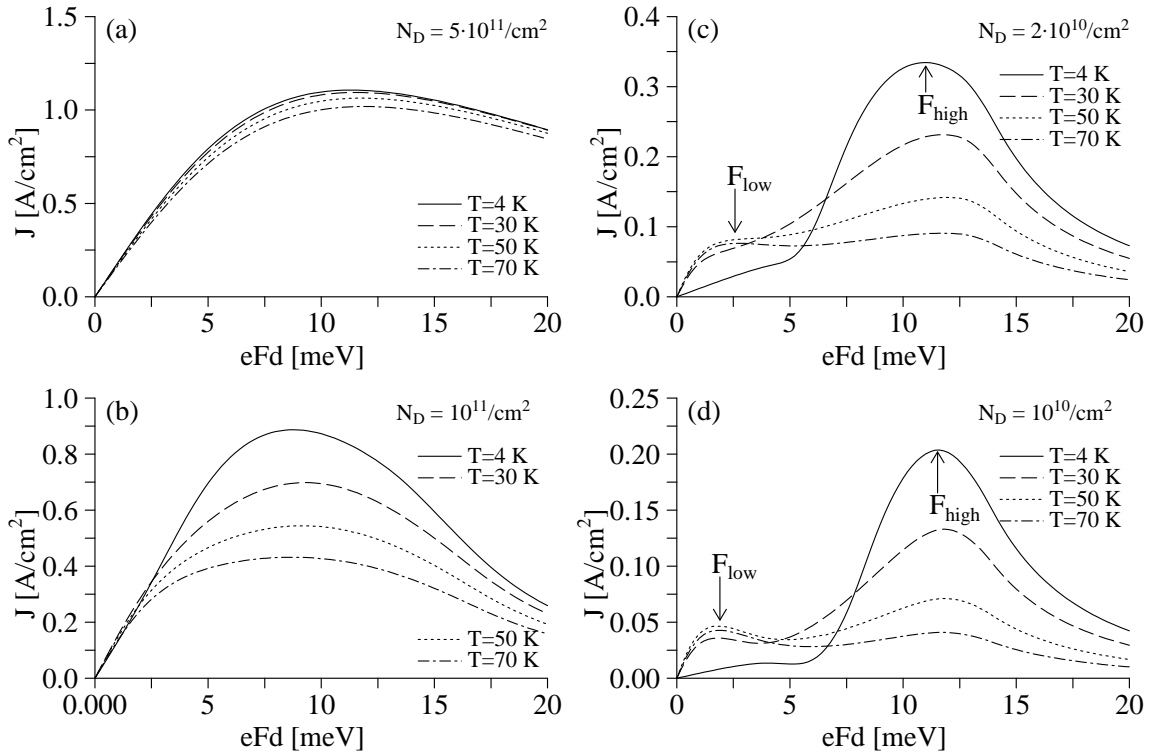


FIG. 7. Calculated temperature dependence of the current-field relations for different doping densities using TF screening.

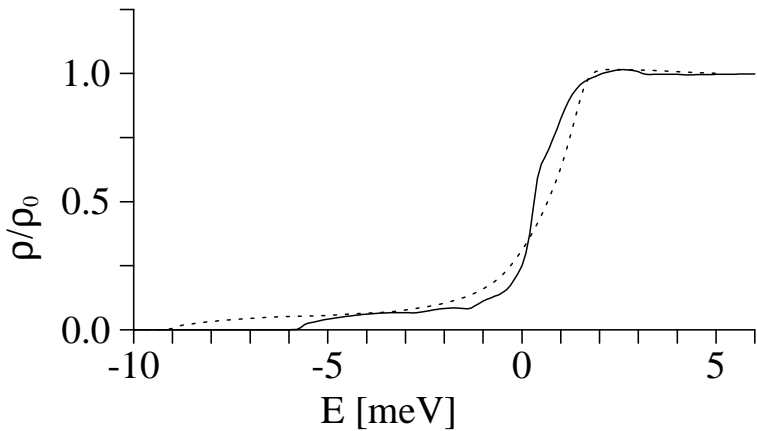


FIG. 8. Calculated density of states for the sample parameters of Ref. [21,22] using RPA screening (full line) and TF screening (dashed line).

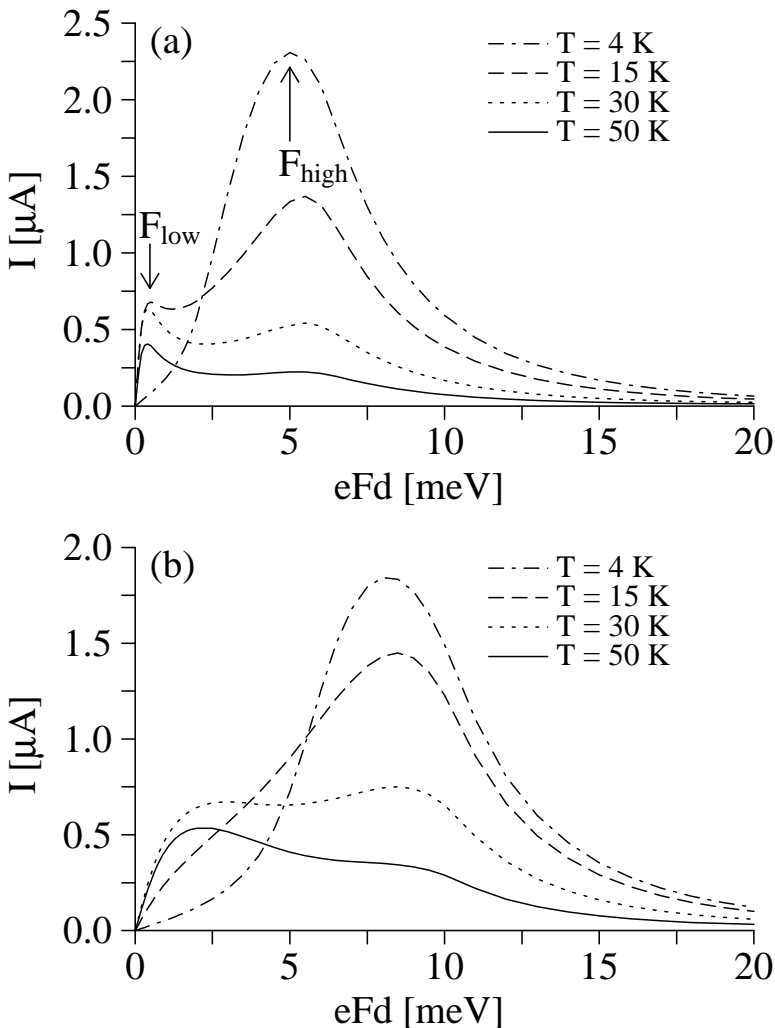


FIG. 9. Calculated temperature dependence of the current-field relations for the sample of Ref. [21,22]. The screening is treated within the RPA (a) and within the Thomas-Fermi approximation (b).

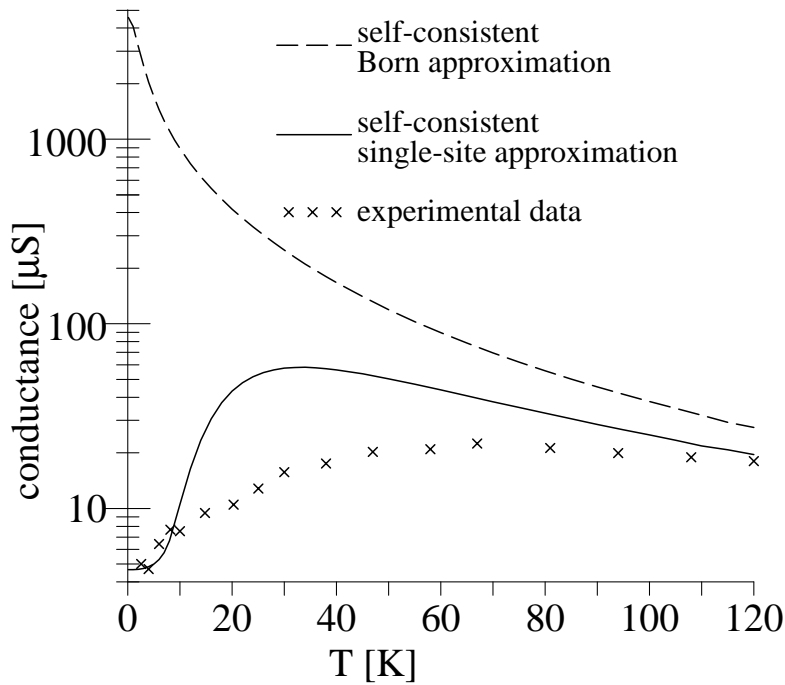


FIG. 10. Temperature dependence of the zero bias conductance for the sample of Refs. [21,22].  
 Full line: Calculation using spectral functions from the single-site approximation and TF screening,  
 dashed line: Calculation using spectral functions from the self-consistent Born-approximation,  
 crosses: experimental data (S. Zeuner and J. Allen, private communication)